

# Considerations about the modeling and simulation of air-gap eccentricity in induction motors

\*A. Ghoggal, A. Aboubou, S. E. Zouzou, M. Sahraoui.

Laboratoire LGEB – Université de Biskra - Algérie

\*Département d'Electrotechnique  
Université Mentouri – Route ain el-bai  
Constantine - 25000 - Algérie  
E-Mail: ghoetudes@yahoo.fr

H. Razik

Groupe de Recherches en Electrotechnique et  
Electronique de Nancy GREEN - UHP - UMR - 7037  
Université Henri Poincaré - Nancy 1 - BP 239  
F - 54506 Vandoeuvre-les-Nancy, Cedex, France  
E-Mail: Hubert.Razik@green.uhp-nancy.fr

**Abstract**— This paper proposes, firstly, a precise evaluation of the inductances of induction machine (IM) by transforming the calculations into a simple calculation of surfaces. The skewing bars effect and linear rise of the magneto-motive force (MMF) across the slot in case of constant or nonuniform air-gap are taken into account. Secondly, we consider the two types of star stator winding coupling of IM, YN-connected and Y-connected. The choice of a 2-pole IM in our application is due to the fact that the majority of the previous publications have used a 4-pole IM or more. Also, and particularly, the 2-pole IM can have homopolar flux in presence of eccentricity or odd number of slots per pole. It is the reason for which it deserves a particular interest. The model is established initially in case of symmetric machine, then, in the frequent case of radial eccentricity which is the mixed eccentricity. This objective would be achieved by exploiting an extension in 2-D of the modified winding function approach (MWFA). The analysis is validated by comparing the experimental line-current spectra of the eccentric machine to the simulation results.

**Index Terms**— Induction machines, inductance, MWFA, space harmonics, skew, air-gap eccentricity.

## I. INTRODUCTION

THE INDUCTION motors play a very important role in efficient running of industrial processes. Premature detection of defects in the motors will help avoid costly failures. It is well known now that rotor faults of IM yield asymmetrical operation of this one, causing unbalanced currents, torque pulsation, vibrations and increased losses. The need for detection of rotor faults at an earlier stage, so that maintenance can be scheduled, has pushed the development of new monitoring methods. In this aim, several studies have showed that higher and lower sidebands frequencies can appear in the stator frequency spectral analysis of the line currents, the torque, the speed and the power [3],[11],[13],[16]. These ones can be a sign of defects. So, in order to study the laws of variation of these indicators, a model closer to reality considering faults conditions to any degree and with a minimum of computation complexity is always required.

In [1],[2] and [4], the winding function approach (WFA) is used to analyse IM faults. It does not initially include the air-gap variation, but if this effect is introduced in the integral giving the total flux, and later on, in the inductance expression, unfortunately, it leads to inequalities between  $L_{sr}$  and  $L_{rs}$ . The MWFA consists in the rearrangement of WFA

to include the air-gap nonuniformity resulting in identical values for  $L_{sr}$  and  $L_{rs}$  [6],[7]. Several diagnosis studies have adopted the MWFA. In these papers, static, dynamic eccentricity and axial nonuniformity are considered on the basis of the modeling of the permeance function of air-gap by an approximated expression [10],[13],[16]. In order to limit the number of expansion terms, the authors of [12] have proposed a geometrical model of IM eccentricity based on the use of  $(p + 1)$  harmonics in the permeance function of the air-gap. Note that without this development, the use of a numerical integration to deduce the inductances is essential, resulting in a heavy calculus burden. As for the modeling of slots skewing, one of the ways is that presented in [9]. It is based on the description of the inductance per unit of length. This supposes that in any radial section of the machine, the mutual inductance per unit of length is constant, i.e. the stator coil and a rotor loop has the same shape, but is displaced in space. In [8],[10], the skew and axial eccentricity are modeled analytically using a 2-D extension of the MWFA.

The present work is focused on the search of appropriate expressions for the inductances of IM taking into account, the rotor skewing bars and air-gap nonuniformities. The proposed technique requires less simulation time than those based on Fourier series of winding turns functions, which requires a great number of expansion terms. Despite the adopted approximations, this approach yields to a huge computational burden, but the advantage is that the derivative of Fourier series is easily obtained. With the proposed method, the overall accuracy is not affected. On the other hand, we show that three phase stator winding YN-connected can generate the principal-slot-harmonics (PSH) associated with a triplen pole pair in the line currents even under balanced supply voltages. The steady-state spectral components of the stator currents obtained both experimentally and by simulation validate these results.

## II. CALCULATION OF THE INDUCTANCES

### A. Curvature radius and polar radius!

Knowing that by including the axial dimension, the turns function  $n$  and the inverse of air-gap function  $g^{-1}$  are defined in comparison to the mechanical position of the rotor measured by respecting a fixed stator reference, and to an axial reference. Thus, one can lead to an extended form of the modified winding function which does not imply any

restriction as for the axial uniformity [10]

$$N(\varphi, z, \theta_r) = n(\varphi, z, \theta_r) - \frac{1}{2\pi \langle g^{-1}(\varphi, z, \theta_r) \rangle} \int_0^{2\pi l} n(\varphi, z, \theta_r) g^{-1}(\varphi, z, \theta_r) dz d\varphi \quad (1)$$

where  $\langle g^{-1}(\varphi, z, \theta_r) \rangle$  is the average value of the inverse of air-gap function. We put forward the following notations. Let  $F$  be the MMF distribution in the air-gap due to the current  $i_{Ai}$  flowing in an arbitrary coil  $Ai$ . Let  $d\phi$  be the elementary flux in the air-gap which is measured in comparison to an elementary volume of section  $ds$  and length  $g$ . Thus, the expression of the elementary flux is given as follows

$$d\phi = \mu_0 F g^{-1} ds, \quad (2)$$

where  $ds = l d\eta$  and  $\eta$  is the limit of the surface  $S$ . In several works, the calculation of the flux  $\phi$  is obtained thanks to the definition of  $S$  and  $ds$ . [5] and [10] suppose that the average radius of the air-gap does not change even in case of eccentricity. However, [12] and [13] introduce the average radius of the air-gap  $r(\varphi, z, \theta_r)$  in case of eccentricity as one variable inside the integral, a way to define the element of surface  $ds$ . In this section, we will inspect how the variation of  $r$  compared to the variation of the air-gap length is negligible. If we want to take highly into account the non-circular section of  $S$ , we must define it using its curvature radius  $R$  instead of the polar radius  $r$  which holds its definition with respect to a fixed point. So, to simplify the idea, we consider that  $r$  does not vary down  $Z$ . For a particular position of the rotor, and by referring to Fig. 1, we can mathematically demonstrate that the length of the arc  $d\eta$  can be obtained by

$$d\eta = \sqrt{(dr)^2 + r^2 (d\varphi)^2} \quad (3)$$

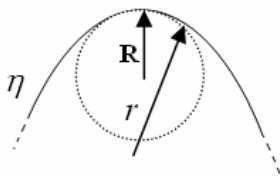


Fig. 1. Representation of the polar radius and the curvature radius in a non circular curve.

$d\eta = rd\varphi$  is verified only if it is supposed that  $dr/d\varphi$  is negligible. Thus,  $r$  is reduced to  $r_0$ . Consequently, we return to the initial case where it is admitted that the variations of the average radius  $r$  in case of eccentricity does not affect the calculations in front of the air-gap variations.

### B. Inductances calculation using a 2-D representation of the induction machine.

As described in [8], and considering the plane representation in 2-D of IM, the expression giving the flux seen by all turns of coil  $Bj$  of winding  $B$  due to current  $i_{Ai}$

flowing in coil  $Ai$  of winding  $A$  will be reduced to:

$$\phi_{BjAi} = \mu_0 \int_{x_{1j}}^{x_{2j}} \int_{z_{1j}(x)}^{z_{2j}(x)} N_{Ai}(x, z, x_r) n_{Bj}(x, z, x_r) g^{-1}(x, z, x_r) i_{Ai} dz dx. \quad (4)$$

Generally, and by taking into account the axial asymmetry,  $n_{Bj}$  and  $N_{Ai}$  could be redefined to describe the slots skewing. Particularly, the rotor bars skewing can be considered by replacing  $Bj$  by a rotor loop  $r_j$  and supposing that  $Ai$  is a stator coil. Fig. 2 depicts the displacement of a rotor loop  $r_j$  under the field of a stator coil  $Ai$ . The skew of the rotor bars is taken into account by the definition of  $z(x)$  in (4) which can describe either uniform or spiral skew. Note that the pitch  $\alpha_{Ai}$  of coil  $Ai$  is defined with respect to its sides placed at  $x_{1i} = r_0 \cdot \varphi_{1i}$  and  $x_{2i} = r_0 \cdot \varphi_{2i}$ . Generally, the total flux  $\psi_{BA}$  relating to all coils (any winding  $A$  and  $B$ ) holds its general expression by integrating over the whole surface. The mutual inductance  $L_{BA}$  is the flux  $\psi_{BA}$  per unit of current. So it yields

$$L_{BA}(x_r) = \mu_0 \int_0^{2\pi r_0 l} \int_0^l N_A(x, z, x_r) n_B(x, z, x_r) g^{-1}(x, z, x_r) dz dx. \quad (5)$$

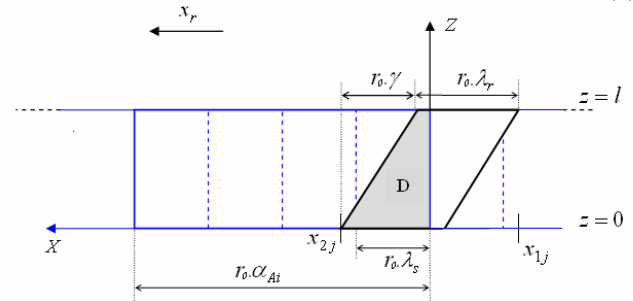


Fig. 2. The rotor bar skewing in 2-D representation.

In order to write subroutines specifically intended for the calculation of the machine inductances, it is possible to deduce an expression which can be easily translated into an algorithm. In this case, using  $g^{-1}(x, z, x_r) = P(x, z, x_r)$ , (1) becomes

$$N_A(x, z, x_r) = n_A(x, z, x_r) - \frac{\langle P \cdot n_A \rangle}{\langle P \rangle}. \quad (6)$$

Substituting (6) into (5) yields

$$L_{BA}(x_r) = 2\pi r_0 l \mu_0 \left( \left( \sum_{i=1}^q \sum_{j=1}^p \langle P n_{Ai} n_{Bj} \rangle \right) - \frac{\langle P n_A \rangle \cdot \langle P n_B \rangle}{\langle P \rangle} \right), \quad (7)$$

where  $q$  and  $p$  are the number of coils of winding  $A$  and  $B$  respectively. Note that  $L_{AB} = L_{BA}$  and that the mutual inductance between  $A$  and  $B$  is a function of mutual inductances of their elementary coils. These elementary mutual inductances depend on the number of turns, their beginning and ending position in the slots, their connection and their polarity. The

resulting algorithm is easily adaptable to any winding. Unlike [2], this approach eliminates look-up tables containing the inductance values.

As an example, (7) will now be used to calculate the mutual inductance between stator winding  $A$  and the rotor loop  $r_j$  considering a uniform air-gap and a skewed rotor bars. According to Fig. 2, the turns functions can be expressed in 2-D like (8) and (9).

$$n_{r_j}(x, z, x_r) = \begin{cases} 1 & x_{1_j} \langle x \langle x_{2_j}, z_{1_j}(x) \langle z(x) \langle z_{2_j}(x). \\ 0 & \text{Otherwise} \end{cases} \quad (8)$$

$$n_{A_i}(x) = \begin{cases} w & x_{1_i} \langle x \langle x_{2_i} \\ 0 & \text{Otherwise} \end{cases} \quad (9)$$

Particularly, when the rotor loop is completely under the field of the stator coil, one can write

$$\langle Pn_{A_i}n_{r_j} \rangle = \frac{1}{2\pi r_0 l g_0} \int_{x_{1_j}(x)}^{x_{2_j}(x)} \int_{x_{1_i}(x)}^{x_{2_i}(x)} n_{A_i}(x) n_{r_j}(x, z, x_r) dz dx, \quad (10)$$

When the rotor loop is partially under the field of the coil, the interval of integration is reduced to the common surface 'D' (grey region in Fig. 2) among the surface of projection of rotor loop  $r_j$  and that of stator coil  $A_i$ . Thanks to (8) and (9), it is obvious that the integral in the remaining interval is null. Consequently

$$\langle Pn_{A_i}n_{r_j} \rangle = \frac{1}{2\pi r_0 l g_0} \iint_D n_{A_i} \times 1 dz dx. \quad (11)$$

If the linear rise of MMF across the slot is neglected, in this case,  $n_{A_i}$  is constant in the region 'D' and is equal to  $w$ . Thus, according to  $S_D(x_r)$  which is the surface delimited by 'D', equation (11) for the coil  $A_i$  can be written as

$$\langle Pn_{A_i}n_{r_j} \rangle = \frac{w S_D(x_r)}{2\pi r_0 l g_0}. \quad (12)$$

The calculation of (12) is made into an independent subroutine. So, it will be possible to find the double sum in (7). As for  $\langle Pn_A \rangle$  and  $\langle Pn_{r_j} \rangle$ , and owing to the fact that they are independent from position  $\theta_r$ , their values can be easily deduced from the two expressions:

$$\langle Pn_A \rangle = \frac{\langle n_A \rangle}{g_0}, \quad (13)$$

$$\langle Pn_{r_j} \rangle = \frac{S_{r_j}}{2\pi r_0 l g_0}, \quad (14)$$

where  $S_{r_j}$  represents the surface of the rotor loop. The calculation of  $L_{r1A}$  is similar to the calculation of the surface  $S_D(x_r)$ . The same procedure is used to calculate the other inductances. Note that for more accuracy, the effect of linear rise of MMF across the slot described in [9] can be

included in the inductance calculation using the same global formulation proposed.

### C. Modeling of the air-gap eccentricity

Using (7), it will be possible to calculate all inductances of the machine where the expression of the inverse function of air-gap can be analytically approximated as:

$$g^{-1}(x, z, x_r) \approx P_0(z) + P_1(z) \cos(x/r_0 - \rho) + P_2(z) \cos(2(x/r_0 - \rho)) \quad (15)$$

$\rho$  and coefficients  $P_0, P_1$  and  $P_2$  are calculated from  $g_0, \delta_s(z), \delta_d(z)$  and  $x_r$  as follow

$$\rho(z) = \arctan\left(\frac{\delta_d(z) \sin(x_r/r_0)}{\delta_s(z) + \delta_d(z) \cos(x_r/r_0)}\right), \quad (16)$$

$$\delta(z) = \sqrt{\delta_s(z)^2 + \delta_d(z)^2 + 2\delta_s(z)\delta_d(z) \cdot \cos(\rho(z))}, \quad (17)$$

$$P_i = 2 \cdot \left(\frac{1}{g_0 \sqrt{1 - \delta(z)^2}}\right) \cdot \left(\frac{1 - \sqrt{1 - \delta(z)^2}}{\delta(z)}\right)^i, \quad i=0,1,2 \quad (18)$$

where  $\delta_s$  and  $\delta_d$  are the amount of static and dynamic eccentricity respectively.

## III. SIMULATION RESULTS

### A. Preamble

It is now clear that the presence of PSH in line current of three-phase IM is primarily dependent on the number of rotor slots and number of fundamental pole pairs of the machine. It was also shown in previous works that only PSH associated to a nontriplen pole pair can be seen ideally with a balanced power supply and in symmetrical conditions. For more learning about this problem, the effect of pole pair and rotor slot numbers on the presence of these harmonics under healthy and eccentric conditions was mainly studied in [16].

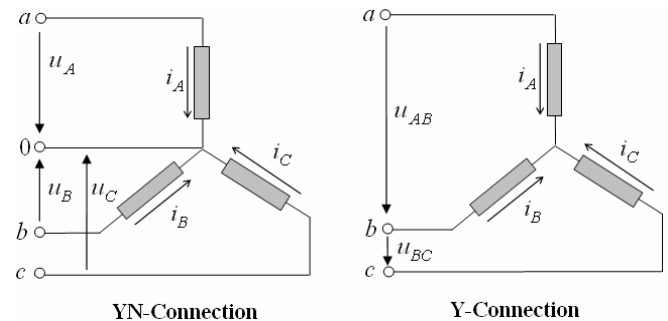


Fig. 3. Stator neutral connection

Awing to the fact that in reality the voltage sum contains extraneous frequencies due to the slot harmonics, inverter drives switching, and load dependence core saturation, we

show that even with a balanced voltage, and by taking into account the slots harmonics, always, there are a non null neutral potential [17],[18]. The connection of the neutral point in YN-connection implies the flowing of a current  $I_n$  between the neutral of the machine and that of the supply, then, the sum of the line currents will not be null (Fig. 3). So, the PSH associated to a triplen pole pair will appear in the line currents spectres.

### B. Inductances calculation

The specific IM studied is a three-phase, 3 kW, 50Hz, 2-pole motor, having four coils per phase, series connected. The other parameters are given in the appendix. Fig. 4 and 5 show the mutual inductance curves between the first stator phase and the first rotor loop, for symmetric case and for the case of mixed eccentricity with three terms used in the development of the inverse of air-gap function. The skew and linear rise of MMF across the slot are taken into account.

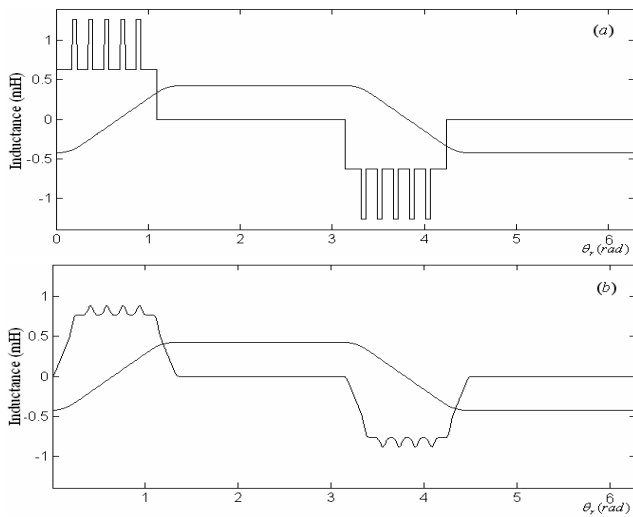


Fig. 4.  $L_{r1A}$  and  $\frac{dL_{r1A}}{d\theta_r}$ , symmetric machine. (a) without skew and slot opening, (b) with skew and slot opening.

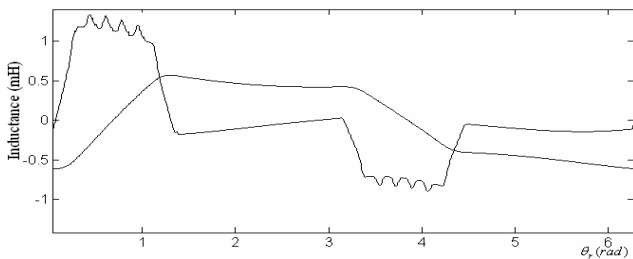


Fig. 5.  $L_{r1A}$  and  $\frac{dL_{r1A}}{d\theta_r}$ , mixed eccentricity of  $\delta_s = 20\%$ ,  $\delta_d = 20\%$ .

### C. Operation under condition of mixed eccentricity

As the squirrel cage can be viewed as identical and equally spaced rotor loops, one can establish voltage and mechanical equations of the loaded IM for a three-phase stator winding YN-connected [1],[2]:

$$\begin{cases} [U] = [R][I] + \frac{d([L][I])}{dt} \\ C_e = [I]^T \cdot \frac{\partial [L]}{\partial \theta_r} \cdot [I] \text{ and } C_e - C_r = J_r \frac{d\omega_r}{dt} \end{cases} \quad (19)$$

$[U]$  corresponds to the system voltages,  $[I]$  to the stator and rotor currents. They are  $(N_b + 4) \times 1$  matrices, where  $N_b$  is the number of rotor bars.  $[R]$  and  $[L]$  are  $(N_b + 4) \times (N_b + 4)$  matrices.  $C_e$  is the electromagnetic torque,  $C_r$  the load torque,  $J_r$  the rotor load inertia, and  $\omega_r$  the mechanical speed of the rotor. In Y-connection, the system must be rearranged as assuring the condition of a null sum of the line currents as described in [1].

Fig. 6 represents the spectra of the line current of the studied IM operating in healthy stat. Each plot is normalised with respect to its fundamental. As shown, the upper and lower PSH can be seen with YN-stator winding connection. The frequencies associated to these harmonics are derived from the general equation given in [15], and described by

$$f_{slot+ecc} = \left[ \left( \frac{N_b \pm n_d}{p} \right) (1-s) \pm 1 \right] \cdot f_s \quad (20)$$

$f_s$  is the main frequency,  $s$  the slip in per unit, and  $n_d = 0$  in static eccentricity, and 1 in dynamic eccentricity. However, only PSH corresponding to the nontriplen pole pair can be seen in case of Y-connection.

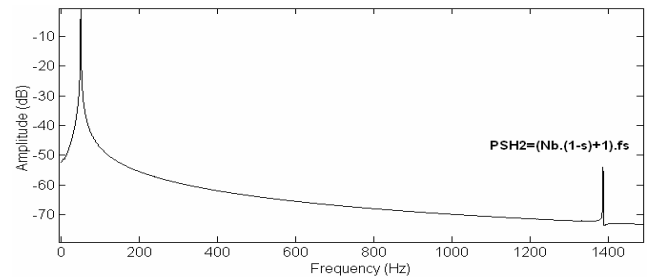
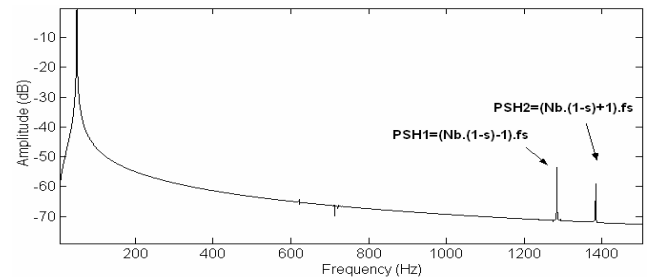


Fig. 6. Stator current spectra in healthy state, YN-connection (top), Y-connection (bottom).  $s=0.045$ .

Fig. 7 shows the simulation results of the operation of the IM under conditions of mixed eccentricity of  $\delta_s = 20\%$ ,  $\delta_d = 20\%$ . In the low range frequency, it is possible to see the low frequency components described by

$$f_{mix} = |f_s \pm k \cdot f_r|, \quad (k = 1, 2, 3 \dots) \quad (21)$$

where  $f_r$  is the rotational frequency of the machine [7],[14]. In the high range frequency, the two PSH and components near the PSH appear when considering YN-connection of the stator winding.

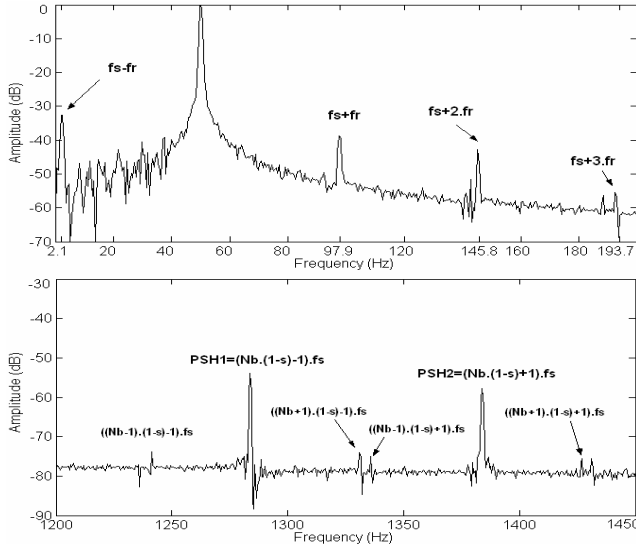


Fig. 7. Stator current spectra with mixed eccentricity condition, YN-connection,  $s = 0.042$ . Low frequencies (top), high frequencies (bottom).

As predicted, when we consider the Y-connection and under balanced supply, only the highest PSH associated to the nontriplen pole pair can be seen (Fig. 8), while the two PSH are generated when considering 5% of supply unbalance (Fig. 9) [16]. The others eccentricity harmonics are very weak.

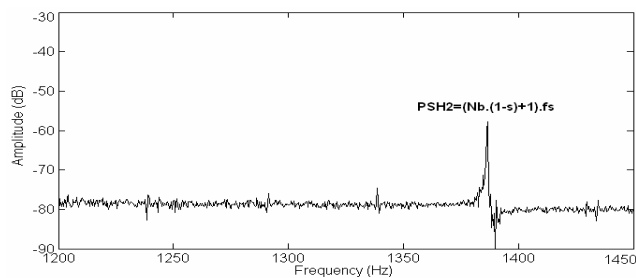


Fig. 8. Stator current spectrum with mixed eccentricity condition, Y-connection,  $s = 0.041$ , high frequencies.

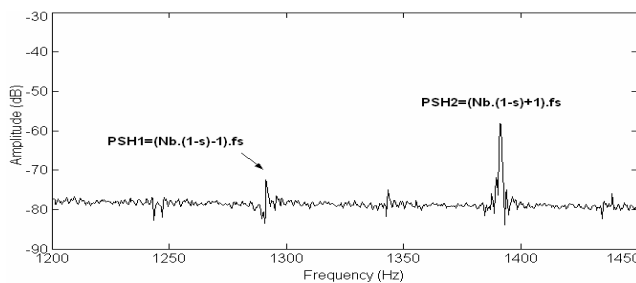


Fig. 9. Stator current spectrum with mixed eccentricity condition and 5% of supply unbalance, Y-connection,  $s = 0.04$ , high frequencies.

## VI. EXPERIMENTAL RESULTS

The experimental tests were carried out on an experimental bench in the Nancy-GREEN laboratory, France. Fig. 10 and 11 show the experimental results of the operation of the same IM used in simulation. The stator winding is Y-connected. The spectra of fig. 10 shows that even in a healthy state, there are always frequency components but of low amplitudes. This is due to the inherent level of eccentricity, by some degree of rotor asymmetry and from noise introduced by the power supply.

A small level of eccentricity was created by replacing the rotor bearings by a set of faulty bearings. Fig. 11 shows that the replacement of the bearings did introduce a small amount of eccentricity.

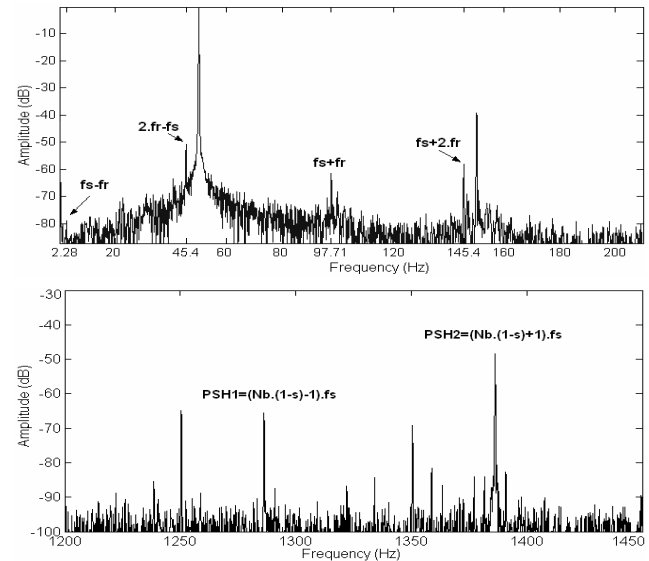


Fig. 10. Stator current spectra in healthy stat,  $s = 0.045$ . Low frequencies (top), high frequencies (bottom).

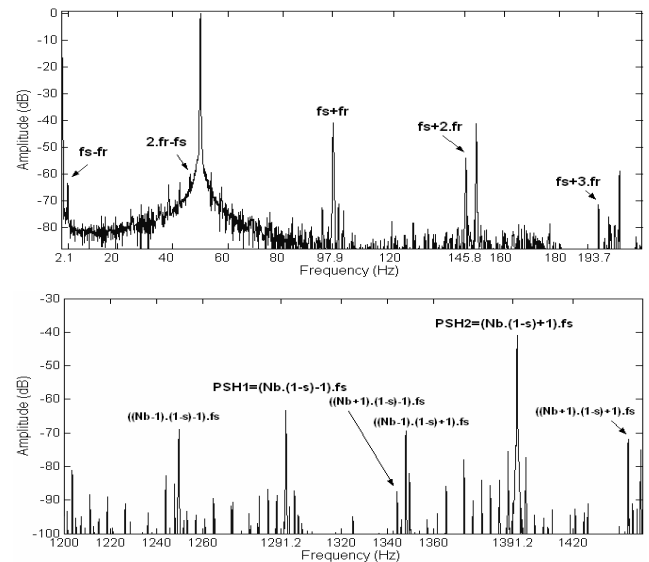


Fig. 11. Stator current spectra with mixed eccentricity condition,  $s = 0.042$ . Low frequencies (top), high frequencies (bottom).

A significant increase of the amplitude of the characteristic frequency components can be easily noticed on both low and high frequency spectrums. Lower and upper sidebands harmonics close to the fundamental show an increase of approximately 20dB. Furthermore, PSH and surrounding frequencies also appear at the exact frequencies predicted by (20). Note that, due to the power supply unbalance, the two PSH are present in the spectra. Also, it has to be remembered that a good diagnosis of mixed eccentricity requires the knowledge of both low and high frequency components.

## V. CONCLUSION

In this work, the MWFA was presented while considering the axial dimension. It was verified that the average radius of the air-gap could be considered invariable even in presence of eccentricity. Under this assumption, a model of IM was established. It proves very useful to study, with more accuracy, others faults operating conditions like broken rotor bars and end-rings [11], the axial eccentricity [8], and which can be extended to study the winding turn-to-turn faults. It was also shown that three phase stator winding YN-connected can generate PSH associated with a triplen pole pair even if the IM is supplied by balanced voltages, although this configuration is seldom used. The steady-state spectral components of the stator currents obtained both experimentally and by simulation confirm that the results are quite satisfactory.

## APPENDIX

### - Machine parameters:

The average air-gap length	: $g_o=0.000172\text{ m}$
Number of rotor bars	: $N_b=28$
Number of stator slots	: $N_e=36$
The average radius of the air-gap in symmetrical condition	: $r_o=0.0516\text{ m}$
Turns per coil	: $w=80$
The length of rotor	: $l=0.125\text{ m}$
Rotor bar leakage inductance	: $L_b = 0.000172H$
Stator phase leakage inductance	: $L_\lambda = 0.009594H$
Stator phase resistance	: $R_s = 2.86\Omega$
Rotor bar resistance	: $R_b = 2.856e-5\Omega$
End ring resistance	: $R_e = 1.8560e-005\Omega$
Moment of inertia	: $J_r = 0.023976\text{ kgm}^2$
Mechanical angle of the skew	: $\gamma = \pi / 14\text{ rad}$
Stator slot opening	: $\beta = \pi / 36\text{ rad}$

## REFERENCES

- [1] X. Luo, Y. Liao, H.A. Toliyat, A. El-Antably and T.A. Lipo, "Multiple coupled circuit modeling of induction machines," *IEEE Trans. Industry Applications*, vol. 31, no. 2, pp. 311-318, Mar./Apr. 1995.
- [2] H.A. Toliyat and T.A. Lipo, "Transient analyse of induction machines under stator, rotor bar and end ring faults," *IEEE Trans. Energy Conversion*, vol. 10, no. 2, pp. 241-247, June 1995.
- [3] H. Henao, H. Razik and G. A. Capolino, "Analytical approach of the stator current frequency harmonics computation for detection of induction machine rotor faults," *IEEE Trans. Industry Applications*, vol. 41, no. 3, pp. 24-34, May/June 2005.
- [4] H.A. Toliyat, M.S. Arfeen and A.J. Parlos, "A method for dynamic simulation of air-gap eccentricity in induction machine," *IEEE Trans. Industry Applications*, vol. 32, no. 4, pp. 910-918, July/August 1996.
- [5] N.A. Al-Nuaim and H.A. Toliyat, "A novel method for modelling dynamic air-gap eccentricity in synchronous machines based on modified winding function theory," *IEEE Trans. Energy Conversion*, vol. 13, no. 2, pp. 156-162, June 1998.
- [6] J. Faiz and I.T. Ardekaneh, "Extension of winding function theory for nonuniform air-gap in electric machinery," *IEEE Trans. Magnetics*, vol. 38, no. 6, pp. 3654-3657, Nov. 2002.
- [7] S. Nandi, R.M. Bharadwaj and H.A. Toliyat, "Performance analyse of three-phase induction motor under mixed eccentricity condition," *IEEE Trans. Energy Conversion*, vol. 17, no. 3, pp. 392-399, Sept. 2002.
- [8] A. Ghoggal, M. Sahraoui, A. Aboubou, S.E. Zouzou and H. Razik, "An Improved Model of the Induction Machine Dedicated to Faults-Detection - Extension of the Modified Winding Function," *In proceeding of IEEE ICIT 2005, Hong-Kong, China, 14-17 Dec. 2005*.
- [9] M.G. Joksimovic, D.M. Durovic and A. B. Obradovic, "Skew and linear rise of MMF across slot modelling-Winding function approach," *IEEE Trans. Energy Conversion*, Vol. 14, no. 3, pp. 315-320, Sept. 1999.
- [10] G. Bossio, C.D. Angelo, J. Solsona, G. Garcia and M.I. Valla, "A 2-D Model of the induction machine: Extension of the modified winding function approach," *IEEE Trans. Energy Conversion*, vol. 19, no. 1, pp. 144-150, Mar. 2004.
- [11] S.E. Zouzou, A. Ghoggal, A. Aboubou, M. Sahraoui and H. Razik, "Modelling of induction machines with skewed rotor slots dedicated to rotor faults," *In proceeding of IEEE Sdemped 2005, Vienna, Austria, 7-9 Sept. 2005*.
- [12] J. Faiz, I.T. Ardekaneh and H.A. Toliyat, "An Evaluation of inductances of squirrel-cage Induction motor under mixed eccentric conditions," *IEEE Trans. Energy Conversion*, vol. 18, no. 2, pp. 252-258, June 2003.
- [13] M.G. Joksimovic, D.M. Durovic, J. Penman and N. Arthur, "Dynamic simulation of dynamic eccentricity in induction machines-Winding function approach," *IEEE Trans. Energy Conversion*, vol. 15, no. 2, pp. 143-148, June 2000.
- [14] D.G. Dorrell, W.T. Thomson and S.Roach, "Analyse of air gap signals as function of combination static and dynamic air gap eccentricity in 3-phase induction motors," *IEEE Trans. Industry Applications*, vol. 33, no. 1, pp. 24-34, Jan./Feb. 1997.
- [15] J.R. Cameron, W.T. Thomson, A.B. Dow, "Vibration and current monitoring for detecting air-gap eccentricity in large induction motors," *IEE*, vol. 133, Pt. B, no. 3, pp 155-163, May 1986.
- [16] S. Nandi, S. Ahmed, H.A. Toliyat, "Detection of rotor slot and other eccentricity related harmonics in a three-phase induction motor with different rotor cages", *IEEE Trans. Energy Conversion*, vol. 16, no. 3, pp. 253-260, Sept. 2001.
- [17] M.A. Cash, T.G. Habetler, G.B. Kliman, "Insulation failure prediction in AC machines using line-neutral voltages," *IEEE Trans. Industry Applications*, vol. 34, no. 6, pp. 1234-1239, Nov./Dec. 1998.
- [18] Yamazaki, S. Shinfuku, "Combined 3-D,2-D Finite Element Analysis of Induction Motors Considering Variation of Neutral Point Potential in Star Connection", *IEEE Trans. Magnetics*, vol. 37, no. 5, pp. 1234-1239, Sep.2001.